# Role of local airsea interaction in fire activity over Equatorial Asia

# Role of local air-sea interaction in fire activity over Equatorial Asia

Jin-Soo Kim[1,2], Su-Jong Jeong[3,4], Jong-Seong Kug[5]*, Mathew Williams[1,2]

[1]School of GeoSciences,
University of Edinburgh, Edinburgh, United Kingdom
[2]National Centre for Earth Observation,
University of Edinburgh, Edinburgh, United Kingdom
[3]Department of Environmental Planning,
Graduate School of Environmental Studies,
Seoul National University, Seoul, South Korea
[4]Institute for Sustainable Development (ISD),
Seoul National University, Seoul, South Korea
[5]Division of Environmental Science and Engineering,
Pohang University of Science and Technology (POSTECH), Pohang, South Korea

Corresponding author: Jong-Seong Kug (jskug@postech.ac.kr)

**Key Points:**

- Strong diversity of fire activity in Equatorial Asia among El Niño events
- Importance of local air-sea interaction on fire activity. Cooler Banda Sea leads drought and stronger fire activity
- Fire activity is sensitively driven by local SST changes due to strong local air-sea interaction in October

This article has been accepted for publication and undergone full peer review but has not been through the copyediting, typesetting, pagination and proofreading process which may lead to differences between this version and the Version of Record. Please cite this article as doi: 10.1029/2019GL085943

**Abstract**

Fire activity in Equatorial Asia shows large interannual variability. Teleconnections by El Niño–Southern Oscillation and Indian Ocean Dipole are linked to drought and fire events; however, we found here that significant role of local Sea Surface Temperature (SST) over the Banda Sea in interannual variability of Equatorial Asian burned area in October even after removing the linear effects of teleconnections. October is the transient period from dry to wet season and strengthened seasonal circulation in October leads to a negative SST anomaly through Wind–Evaporation–SST mechanism. This anomalous local air-sea interaction sustains the dry season into October and stronger fire activity. Moreover, we found that the sensitivity of precipitation to SST is higher in October than in other months, hence fires in Equatorial Asia can be sensitively driven by local SST changes. Identification of this sensitivity will underpin better predictions of fire activity and air quality in Equatorial Asia.

**Plain Language Summary**

Previous studies have emphasized the remote forcing associated with El Niño–Southern Oscillation and Indian Ocean Dipole are the most important climate factors in controlling fire activity in Equatorial Asia. However, we found here that there is a huge diversity of fire activity among El Niño events. In this paper, we newly found that the local air-sea interaction significantly influences on fire activity in Equatorial Asia. When the seasonal wind gets stronger, the Banda Sea, local sea located between Kalimantan and New Guinea, is cooler and it leads to the drought and strong fire activity. We also found that the role of local air-sea interaction strongly depends on the seasonality, which is related to seasonal variation of sea surface temperature climatology. Our findings will be utilized for better predictions of fire activity and air quality in Equatorial Asia.

## 1. Introduction

The global total of annual summation of fire emissions was 2.17 PgC $yr^{-1}$ (95% confidence interval: 2.04–2.33 PgC $yr^{-1}$) over 1997–2015 period (van der Werf et al., 2017), while fossil fuel and cement emissions were 8.28 PgC $yr^{-1}$ for the same period (Le Quéré et al., 2016). Substantial interannual variability of global fire emissions originates from fire emissions over Equatorial Asia (van de Werf et al., 2004; van de Werf et al., 2008). This region shows the largest confidence interval of mean fire emissions, 0.09–0.30 PgC $yr^{-1}$ at 95% confidence level based on the bootstrap method (Figure 1a). Forest and peatland fires in Indonesia generate most of the fire activity in Equatorial Asia, especially in eastern Sumatra, southern Kalimantan and southern New Guinea (Figure 1b). In addition to substantial carbon emissions, Indonesian fires lead to hazardous levels of smoke pollution over Equatorial Asia and are linked to multitudinous premature deaths (Gaveau et al., 2014; Crippa et al., 2016; Koplitz et al., 2016).

Equatorial Asian fires generally break out in dry season, August to October. Interannual variability of fires is closely related to local drought in that season and tightly coupled to large-scale atmospheric circulation anomaly in the tropics, such as El Niño–Southern Oscillation (ENSO) and Indian Ocean Dipole (IOD) (Field & Shen, 2008; Field et al., 2009; Pan et al., 2018). Walker circulation is weakened during El Niño, accompanying negative sea surface temperature anomalies (SSTA) surrounding Indonesia and eastward shifts of atmospheric convection into the central Pacific, in contrast to positive SSTA and precipitation anomaly in the eastern Pacific (Hendon, 2003). The positive phase of the IOD is also characterized by cold water along the Sumatran coast related to anomalous wind-driven upwelling and less precipitation over Equatorial Asia (Saji et al., 1999). This precipitation variation leads to fire-prone conditions linked to large-scale atmospheric circulation anomaly (Field & Shen, 2008; Field et al., 2009). Thus, year-to-year variation of fire activity in Equatorial Asia is predictable

on seasonal timescales based on using large-scale SSTA patterns related to ENSO and IOD. (Chen et al., 2016b).

The estimated maximum annual carbon emission over Equatorial Asia during 1995–2015 was 1.11 PgC $yr^{-1}$ in 1997 due to severe drought resulting from the 1997/98 El Niño. This El Niño was regarded as one of the strongest events in the historical record (Page et al., 2002; van der Werf et al., 2017). The SSTA in recent 2015/16 El Niño tied with 1997/98 El Niño as the strongest; however, carbon emissions from equatorial fires in 2015, 0.40 PgC $yr^{-1}$, were relatively less than the 1997/98 case (Liu et al., 2017a; Wang et al., 2018). Even though the 2015/16 case had a similar tropical Pacific SSTA magnitude to 1997/98, the IOD event was relatively weaker in 2015/16 than 1997/98 (Chen et al., 2016a; Liu et al., 2017b). Indeed, distinct El Niño types have been reported based on the spatial pattern of SSTA, such as Eastern Pacific El Niño and Central Pacific El Niño (Ashok et al., 2007; Kao and Yu, 2009; Kug et al., 2009). In addition, each El Niño has diverse atmospheric teleconnections related to SSTA diversity of El Niño events (Larkin & Harrison, 2005; Weng et al., 2007, 2009; Kug et al., 2010; Kim & Kug, 2019) and interaction with other basin variabilities (Kug & Kang, 2006; Ham et al., 2003; Park et al., 2018). Even though El Niño phenomenon has a conventional characteristic as positive SSTA in the tropical Pacific, each El Niño is not occurred always same and it shows diverse characteristics in terms of spatial and temporal evolutions, magnitude, and its atmospheric teleconnections (Wang et al., 2019), therefore we expect this El Niño diversity would affect the year-to-year variation of fire activity in Equatorial Asia.

Our science question here is how El Niño diversity drives the interannual variation of fire activity in Equatorial Asia. We analyze fire activity in Equatorial Asia for its connection to ENSO, IOD and local SSTA surrounding Indonesia. Based on this preliminary analysis, we investigate air-sea interactions over the local sea region, to determine their importance for the

interannual variability of fire activity in Equatorial Asia. The novelty of this paper is in the focus on local air-sea interactions with fire.

## 2. Data

The fourth version of Global Fire Emissions Database (GFED4) burned area product with 0.25° × 0.25° resolution is used to quantify the interannual variability of fire over Equatorial Asia (90°E–155°E, 11°S–9°N) for the period June 1995 to December 2015 (Giglio et al., 2013). The Met Office Hadley Centre sea Ice and Sea Surface Temperature data version 1 (HadISST1) on a 1° latitude–longitude grid (Rayner et al., 2003) are used in this study. Based on HadISST1, we drive detrended and normalized SSTA-based indices which are Niño3.4 index and Dipole Mode Index (DMI). Niño3.4 is the average SST anomaly in the region bounded by 170°W–120°W, from 5°S–5°N. The DMI is defined by SSTA gradient between the western equatorial Indian Ocean (50°E–70°E, 10°S–10°N) and the southeastern equatorial Indian Ocean (90°E–110°E, 10°S–0°N) (Saji et al., 1999). In order to examine relationship between fire activity and large-scale atmospheric circulation, the monthly 10-meter zonal and meridional wind and precipitation rate for 1979–2015 are obtained from the European Centre for Medium-Range Weather Forecasts Reanalysis-Interim on a 1.5° latitude–longitude grid (Dee et al., 2011) and from the Climate Prediction Center Merged Analysis of Precipitation on a 2.5° latitude–longitude grid (CMAP; Xie & Arkin, 1997), respectively. GFED4 burned area product only covers recent 21-years period, but we used the whole period of atmospheric variables in order to draw more confidential results with larger sample size.

## 3. Methods and Results

### 3.1 Equatorial Asia Fire Diversity

Niño3.4 index and DMI have been used to explain and predict fire activity in Equatorial Asia because ENSO and IOD are major components in driving Equatorial Asia weather conditions (Field & Shen, 2008; Wooster et al., 2012; Chen et al., 2016b). Field et al. (2009) suggested that a combined index based on monthly Niño3.4 and DMI, Niño3.4-DMI index, better explains the interannual variability of Indonesian precipitation than either Niño3.4 or DMI alone. Monthly Niño3.4-DMI index can be calculated based on multiple linear regression method, which is expressed below:

$$\text{Burned area} = \alpha \cdot \text{Niño3.4} + \beta \cdot \text{DMI} \ + \varepsilon \qquad (1)$$

$$\text{Burned area} - \varepsilon = \alpha \cdot \text{Niño3.4} + \beta \cdot \text{DMI} = \gamma \cdot \text{Normalized Niño3.4-DMI index} \qquad (2)$$

where burned area is monthly total summation of burned area over Equatorial Asia (90°E–155°E, 11°S–9°N), $\alpha$ and $\beta$ are multiple regression coefficients with respect to normalized monthly Niño3.4 and DMI and $\varepsilon$ is a residual. In other words, monthly Niño3.4-DMI index is defined by a summation of partial contributions with respect to normalized Niño3.4 and DMI on Equatorial Asian burned area (Field et al., 2009) and $\gamma$ in equation (2) is standard deviation of monthly Niño3.4-DMI index. Monthly Niño3.4-DMI-related fire activity, $\gamma$, shows distinctive seasonal cycle with the major peak in boreal autumn and the minor peak in boreal spring (Figure 2). Partial contribution of the burned area with Niño3.4, $\alpha \cdot \text{Niño3.4}$ in equation (1), follow the seasonal pattern of the Niño3.4-DMI index; however, the maximum for partial contribution with DMI, $\beta \cdot \text{DMI}$ in equation (1), is in October and it is higher than $\alpha \cdot$Niño3.4 in October and November, possibly because the Indian Ocean dipole peaks in October and November. It means that the Indian Ocean dipole also has a substantial role in the fire activity together with Niño3.4 as consistent with previous studies (Field et al., 2009; Pan

et al., 2018). We found that correlations between burned area and Niño3.4-DMI index are significant for all months. However, residuals, $\varepsilon$ in equation (1), which could not be explained by the Niño3.4-DMI index, still have considerable amounts.

This residual might originate from diverse responses to different characteristics among El Niño events, and other components' contributions. In order to estimate how much the fire activity is different among inter-El Niño events, we calculated the standard deviation of the residual only for recent seven El Niño events (1997, 2002, 2004, 2006, 2009, 2014 and 2015) which were defined when the normalized Niño3.4 SSTA during December–February was greater than 1 K. As shown in Fig. 2, the standard deviation of residuals for recent seven El Niño years generally follows $\gamma$ and $\alpha$, suggesting that stronger magnitudes of El Niño impacts are linked to larger residuals. Interestingly, however, the maximum amplitude of the residual is in October, while the ENSO impacts show the maximum in September. These results suggest that the responses of the fire activity to El Niño forcing are most diverse in October. Interestingly, we found that normalized local SSTA over the Banda Sea (120°–130°E, 10°–0°S) tends to be more negative in case of stronger fire activity years among El Niño events (Figure S1). During these events under strong negative local SSTA condition, the actual burned area tended to be higher than the explained burned area by regression fitting value based on the Niño3.4-DMI index. However, more positive local SSTA is observed with lesser than expected burned area using empirical regression line based on Niño3.4-DMI index. For example, in 2002 and 2009 the fire activity is lesser than the regression line between Niño3.4-DMI and burned area, and SST anomalies are weaker over the Banda Sea. In contrast, fire activities are higher than the regression line in case of 2004 and 2014, when negative local SST anomalies show a certain degree (−0.8 to −1.1°C). Even though the interannual variability of the burned area follows by Niño3.4-DMI index to a certain degree, it is suggested that local SSTA also have a role in fire activity during El Niño years. This result implies that local SSTA and its relevant

climate condition can also contribute to Equatorial Asian fire activity in addition to large-scale teleconnection influence in the tropics.

### 3.2 Local SST Impacts on Fire activity

To understand the diverse response of the Equatorial Asian fire to El Niño, we need to know what other factors affect the residual. In order to find them, we calculated a partial regression of the gridded SST with the Equatorial Asia burned area index for October after linearly removing the effect of Niño3.4-DMI index, which is express below:

$$\text{Burned area} = \gamma \cdot \text{Niño3.4-DMI} + \delta \cdot \text{Gridded SSTA} + \varepsilon \quad (3)$$

where $\gamma$ and $\delta$ are multiple regression coefficients with respect to normalized Niño3.4-DMI index and SSTA in each grid for October, and $\delta$ is shown in Figure 3a. The fire activity in October is related to surface cooling in the Southern Hemisphere and surface warming in the Northern Hemisphere over the surrounding seas of Equatorial Asia (Figure 3a). This north-south dipole pattern of the correlation might be linked to a co-varying atmospheric circulation. Interestingly, the partial regression shows strong relationship with SST in the Banda Sea (120°–130°E, 10°–0°S). This sea is the nearest regions in which the strongest fire activity is occurring, as shown in Fig. 1b. This result indicates that the local cold sea surface can provide a favorable condition for vigorous fire activity.

In order to understand how the local SST affects the fire activity, we calculate the relationship between normalized local SSTA over the Banda Sea (120°–130°E, 10°–0°S) and gridded precipitation over the Maritime Continent, after removing ENSO and IOD effects (Figure 3b), which is express below:

$$\text{Local SSTA index} = \gamma \cdot \text{Niño3.4-DMI} + \delta \cdot \text{Gridded Precipitation} + \varepsilon \quad (4)$$

where $\gamma$ and $\delta$ are multiple regression coefficients with respect to normalized Niño3.4-DMI index and precipitation anomaly in each grid, and $\delta$ is shown in Figure 3b. It is evident that

the SSTs in the Marginal Seas of Indonesia are positively correlated to local precipitation, consistent with the previous study (Aldrian and Susanto 2003). This positive relation indicates that SST variability tends to induce local convective response there as pointed out by previous studies (Aldrian and Susanto 2003; Hendon, 2003), rather than the convective activity leading to the SST change. This result supports the expectation that the negative SST anomalies over the Marginal Seas of Indonesia suppress convective activity, leading to severe drought in the dry season.

Even though El Niño and positive phase of IOD are related to negative SSTA over the Banda Sea, local SSTA can be also affected by local air-sea interaction. Figure 3c shows the atmospheric circulation pattern associated with the SST variation over the Banda Sea after removing the effect of normalized Niño3.4-DMI index as same as equation (3). It is clear that this local SST cooling is linked to the anomalous southeasterly wind which is the same direction with climatological wind. This wind anomaly indicates enhancement of the wind speed, which induces evaporative cooling of SST, suggesting a strengthening seasonal monsoon pattern described by Chang et al. (2005), Iskandar (2010), Kubota et al. (2011) and Hamada et al. (2012).

The correlation between burned area with local SSTA in October is the highest among SSTA-based indices (Table 1). Also, partial correlations without local SST are non-significant. Therefore we should consider local SSTA as important for understanding the interannual variation of fire activity in Equatorial Asia, in addition to large-scale teleconnections such as the ENSO and IOD. However, this mechanism is only found in October, and not in September which has the maximum fire activity over Equatorial Asia (Table 1). Indeed, the coldest season in this area is July–September due to SST cooling by wind-driven evaporation, that is, Wind–Evaporation–SST mechanism described by Xie & Philander (1994), as a part of seasonality (Kida & Richards, 2009). Also, seasonal cycle of precipitation also has the minimum in this

period due to the suppression of convection linked to the coldest SST (Field & Shen, 2008). However, as SST is getting warmer by weakening wind-driven evaporation after August, the relationship between SST and precipitation is changing with climatological mean value of SST (Figure 4).

Previous studies argued that there is the non-linear relationship between SST and convection in the tropics (Graham & Barnett, 1987; Waliser & Graham, 1993; Lau et al., 1997). In dry seasons over Equatorial Asia, precipitation is positively correlated to local SST, but not in the wet season (Haylock & McBride, 2001; Aldrian & Susanto, 2003; Hamada et al., 2012), indicating the sensitivity of precipitation to SST is related to the climatological SST. As shown in Figure 4, if the SST is lower than a certain degree (approximately 29°C), the precipitation is positively correlated to the SST, but this relationship can break down if SST is higher, consistent with Lau et al. (1997). The sensitivities of precipitation to SST increase according to the seasonal variation of SST climatology from August to November (Figure 4). The sensitivity is weak when SST is too low, as in August (1.96 mm $d^{-1}$ $°C^{-1}$), but it becomes stronger as the climatological SST becomes higher, reaching 3.79 mm $d^{-1}$ $°C^{-1}$ in October. The sensitivity of precipitation to SST is highest in October and November, suggesting the interannual variation of local SST in October has a significant role in precipitation variation, which is directly associated with fire activity over Equatorial Asia. However, in December, the sensitivity of precipitation to SST breaks down, like in August, due to too high climatological SST.

In addition to the total burned area in Equatorial Asia, we also analyzed the burned area at 1° × 1° latitude-longitude grid scale to quantify a relative role of local SST on regional scale fire activity as compared to Niño3.4 and DMI. Contributions of Niño3.4, DMI and local SST on October burned area over Equatorial Asia are driven by multiple linear regression (Figure S2). Niño3.4 index explains burned area over the southern part of New Guinea (Figure S2a)

and DMI has a larger contribution in the eastern part of Sumatra than Niño3.4 (Figure S2b). On the other hand, fire activity in the southern part of Kalimantan, which has the largest fire activity over Equatorial Asia, mainly associates with the interannual variation of local SST (Figure S2d). In addition, the contribution of local SST on October burned area is larger than the contribution of the Niño3.4-DMI index (Figure S2c), especially for the southern part of Kalimantan. Therefore, local SST impacts must not be overlooked if we are to understand the interannual variation of fire activity in Equatorial Asia, especially for October.

## 4. Concluding Remarks

Large-scale atmospheric circulation changes such as ENSO and IOD have been considered to explain interannual variability of fire in Equatorial Asia, but we found here that the local SST over the Banda Sea in October is also important for explaining drought-related fire activity in Equatorial Asia. We found that diverse fire responses to ENSO or IOD are caused by local air-sea interaction status which is known as Wind–Evaporation–SST mechanism (Xie & Philander, 1994; Kida & Richards, 2009). In addition, the high sensitivity of precipitation to SST contributes to occurrence of drought even for a weak negative SSTA over the Banda Sea. For this diverse local sea response to ENSO or IOD, there is a possibility that various El Niño flavors may contribute to diverse atmospheric circulation and air-sea interaction changes over the Equatorial Asia region (Larkin & Harrison, 2005; Kug et al., 2009; Kug et al., 2010; Capotondi et al., 2015; Kim & Kug, 2019). For example, less fire activity in 2015/16 El Niño as compared to 1997/98 El Niño implies diverse fire response to El Niño flavors (Chen et al., 2016a; Field et al., 2016; Liu et al., 2017a; van der Werf et al., 2017; Wang et al., 2018). Even though August to October mean Niño3.4 indices have equal magnitude as 2.1°C for 1997/98 and 2015/16 El Niño, 2015/16 has stronger SSTA over the central Pacific and less dry condition over Equatorial Asia than 1997/98 (Chen et al., 2016a; Lim et al., 2017). Moreover, October

Banda Sea SSTA is −0.36°C in 2015/16, while −0.63°C in 1997/98. Therefore, less precipitation due to negative local SSTA might contribute to stronger fire activity in 1997/98 as compared to 2015/16, even though El Niño strength is similar. In contrast to El Niño diversity, fire activity has less diversity among La Niña events than El Niño events and this is consistent with less La Niña diversity in terms of spatial pattern in SSTA as shown in Kug & Ham (2011).

Previous studies suggested that statistical models using SSTA-based indices enable to understand predict fire activity (Field & Shen, 2008; Field et al., 2009; Chen et al., 2011; Wooster et al., 2012; Chen et al., 2016b). In addition to basin-scale SSTA-based indices, the local SSTA would be useful for forecasting fire activity, particularly in October, because local SSTA have more significant lagged relationships with burned area in October over Equatorial Asia than for one month before (September; $r$=−0.75) and two months before (August; $r$=−0.65). We found that correlation coefficients between burned area in October and local SSTA in September without Niño3.4 and IOD effects are −0.44 and −0.50, respectively. This result implies that local SSTA in one and two preceding months can be used for October fire activity prediction and it provides higher skill than Niño3.4-DMI index. Moreover, the current seasonal forecasting models have considerable prediction skills, especially for regional Maritime Continent SST and precipitation (Zhang et al., 2016); therefore, the local SSTA simulations by seasonal forecasting models also useful to predict Equatorial Asia fire activity in October. On the other hand, even though the current Earth System Models simulate process-based fire activity, they underestimate ENSO-related fire activity (Kim et al., 2016; Kim et al., 2017). Therefore, we need further investigations into the role of local SSTA-related fire activity under greenhouse warming in terms of the long-term carbon cycle (Yin et al., 2016).

**Acknowledgements**

J.-S. Kim and M. Williams were supported by the United Kingdom Space Agency (Grant Forests 2020) and Natural Environment Research Council of United Kingdom through the National Centre for Earth Observation. S.-J. Jeong was supported by 'R&D Program for Forest Science Technology (Project No. 2019156A00-1921-0101)' provided by Korea Forest Service (Korea Forestry Promotion Institute). J.-S. Kug was supported by the National Research Foundation of Korea (NRF-2018R1A5A1024958). Burned area data are obtained from the fourth version of Global Fire Emissions Database (https://www.globalfiredata.org/data.html). SST data is downloaded online (https://www.metoffice.gov.uk/hadobs/hadisst/). The monthly 10-meter zonal and meridional wind and precipitation rate are obtained from the European Centre for Medium Range Weather Forecasts Reanalysis-Interim (https://apps.ecmwf.int/datasets/) and from the Climate Prediction Center Merged Analysis of Precipitation (https://www.esrl.noaa.gov/psd/data/gridded/data.cmap.html), respectively.

**References**


1. Aldrian, E., & Susanto, R. D. (2003). Identification of three dominant rainfall regions within Indonesia and their relationship to sea surface temperature. *International Journal of Climatology*, *23*, 1435–1452. https://doi.org/10.1002/joc.950
2. Ashok, K., Behera, S. K., Rao, S. A., Weng, H., & Yamagata, T. (2007). El Niño Modoki and its possible teleconnection. *Journal of Geophysical Research: Oceans*, *112*, C11007, doi:10.1029/2006JC003798.
3. Capotondi, A., Wittenberg, A. T., Newman, M., Lorenzo, E. D., Yu, J. Y., Braconnot, P., et al. (2015). Understanding ENSO diversity. *Bulletin of the American Meteorological Society*, *96*, 921–938. https://doi.org/10.1175/BAMS-D-13-00117.1
4. Chang, C.-P., Wang, Z., McBride, J., & Liu, C.-H. (2005). Annual cycle of Southeast Asia—Maritime Continent rainfall and the asymmetric monsoon transition. *Journal of Climate*, *18*, 287–301. https://doi.org/10.1175/JCLI-3257.1
5. Chen, C.-C., Lin, H.-W., Yu, J.-Y., & Lo, M.-H. (2016a). The 2015 Borneo fires: what have we learned from the 1997 and 2006 El Niños? *Environmental Research Letters*, *11*, 104003. https://doi.org/10.1088/1748-9326/11/10/104003
6. Chen Y., Morton, D. C., Andela, N., Giglio, L., & Randerson, J. T. (2016b). How much global burned area can be forecast on seasonal time scales using sea surface temperatures? *Environmental Research Letters*, *11*, 045001. https://doi.org/10.1088/1748-9326/11/4/045001
7. Chen, Y., Randerson, J. T., Morton, D. C., DeFries, R. S., Collatz, G. J., Kasibhatla, P. S., et al. (2011). Forecasting fire season severity in South America using sea surface temperature anomalies. *Science*, *334*, 787–791. https://doi.org/10.1126/science.1209472

8. Crippa, P., Castruccio, S., Archer-Nicholls, S., Lebron, G. B., Kuwata, M., Thota, A., et al. (2016). Population exposure to hazardous air quality due to the 2015 fires in Equatorial Asia. *Scientific Reports*, *6*, 37074. https://doi.org/10.1038/srep37074
9. Dee, D. P., Uppala, S. M., Simmons, A. J., Berrisford, P., Poli, P., Kobayashi, S., et al. (2011). The ERA-Interim reanalysis: Configuration and performance of the data assimilation system. *Quarterly Journal of the Royal Meteorological Society*, *137*, 553–597. https://doi.org/10.1002/qj.828
10. Field, R. D., & Shen, S. S. P. (2008). Predictability of carbon emissions from biomass burning in Indonesia from 1997 to 2006. *Journal of Geophysical Research: Biogeosciences*, *113*, G04024. https://doi.org/10.1029/2008JG000694
11. Field, R. D., van der Werf, G. R., Fanin, T., Fetzer, E. J., Fuller, R. Jethva, H., et al. (2016). Indonesian fire activity and smoke pollution in 2015 show persistent nonlinear sensitivity to El Niño-induced drought. *Proceedings of the National Academy of Sciences of the United States of America*, *113*, 9204–9209. https://doi.org/10.1073/pnas.1524888113
12. Field, R. D., van der Werf, G. R., & Shen, S. S. P. (2009). Human amplification of drought-induced biomass burning in Indonesia since 1960. *Nature Geoscience*, *2*, 185–188. https://doi.org/10.1038/ngeo443
13. Gaveau, D. L. A., Salim, M. A., Hergoualc'h, K., Locatelli, B., Sloan, S., Wooster, M., et al. (2014). Major atmospheric emissions from peat fires in Southeast Asia during non-drought years: Evidence from the 2013 Sumatran fires. *Scientific Reports*, *4*, 6112. https://doi.org/10.1038/srep06112
14. Giglio, L., Randerson, J. T., & van der Werf G. R. (2013). Analysis of daily, monthly, and annual burned area using the fourth-generation global fire emissions database

(GFED4). *Journal of Geophysical Research: Biogeosciences*, *118*, 317–328. https://doi.org/10.1002/jgrg.20042

15. Graham, N. E., & Barnett, T. P. (1987). Sea surface temperature, surface wind divergence, and convection over tropical oceans. *Science*, *238*, 657–659. https://doi.org/10.1126/science.238.4827.657
16. Hamada, J.-I., Mori, S., Kubota, H., Yamanaka, M. D., Haryoko, U., Restari, S., et al. (2012). Interannual rainfall variability over northwestern Jawa and its relation to the Indian Ocean Dipole and El Niño-Southern Oscillation events. *Scientific Online Letters on the Atmosphere*, *8*, 69–72. https://doi.org/10.2151/sola.2012-018
17. Haylock, M., & McBride, J. (2001). Spatial coherence and predictability of Indonesian wet season rainfall. *Journal of Climate*, *14*, 3882–3887. https://doi.org/10.1175/1520-0442(2001)014<3882:SCAPOI>2.0.CO;2
18. Hendon, H. (2003). Indonesia rainfall variability: Impacts of ENSO and local air-sea interaction. *Journal of Climate*, *16*, 1775–1790. https://doi.org/10.1175/1520-0442(2003)016<1775:IRVIOE>2.0.CO;2
19. Iskandar, I. (2010). Seasonal and interannual patterns of sea surface temperature in Banda Sea as revealed by self-organizing map. *Continental Shelf Research*, *30*, 1136–1148. https://doi.org/10.1016/j.csr.2010.03.003
20. Kao, H.-Y., & Yu, J.-Y. (2009). Contra sting eastern-Pacific and central-Pacific types of ENSO. *Journal of Climate*, *22*, 615–632. https://doi.o rg/10.1175/2008JCLI2309.1
21. Kida, S., & Richards, K. J. (2009). Seasonal sea surface temperature variability in the Indonesian Seas. *Journal of Geophysical Research: Oceans*, *114*, C06016. https://doi.org/10.1029/2008JC005150
22. Kim, J.-S., Kug, J.-S., Yoon, J.-H., & Jeong, S.-J. (2016). Increased atmospheric $CO_2$ growth rate during El Niño driven by reduced terrestrial productivity in the CMIP5

ESMs. *Journal of Climate*, *29*, 8783–8805. https://doi.org/10.1175/JCLI-D-14-00672.1

23. Kim, J.-S., & Kug, J.-S. (2019). Role of off-equatorial SST in El Niño teleconnection to East Asia during El Niño decaying spring. *Climate Dynamics*, *52*, 7293–7308. https://doi.org/10.1007/s00382-016-3473-0
24. Kim, J.-S., Kug, J.-S., & Jeong, S.-J. (2017). Intensification of terrestrial carbon cycle related to El Niño–Southern Oscillation under greenhouse warming. *Nature Communications*, *8*, 1674. https://doi.org/10.1038/s41467-017-01831-7
25. Koplitz, S. N., Mickley, L. J., Marlier, M. E., Buonocore, J. J., Kim, P. S., Liu, T., et al. (2016) Public health impacts of the severe haze in Equatorial Asia in September–October 2015: demonstration of a new framework for informing fire management strategies to reduce downwind smoke exposure. *Environmental Research Letters*, *11*, 94023. https://doi.org/10.1088/1748-9326/11/9/094023
26. Kubota, H., Shirooka, R. & Hamada, J. I. (2011). Interannual rainfall variability over the eastern Maritime Continent. *Journal of the Meteorological Society of Japan*, *89A*, 111–122. https://doi.org/10.2151/jmsj.2011-A07
27. Kug J.-S., Ahn, M.-S., Sung, M.-K., Yeh, S.-W., Min, H.-S., & Kim, Y.-H. (2010). Statistical relationship between two types of El Niño events and climate variation over the Korean Peninsula. *Asia-Pacific Journal of Atmospheric Sciences*, 46, 467–474. https://doi.org/10.1007/s13143-010-0027-y
28. Kug, J.-S., & Ham, Y.-G. (2011). Are there two types of La Nina events? *Geophysical Research Letters*, *38*, L16704. https://doi.org/10.1029/2011GL048237
29. Kug, J.-S., Jin, F.-F., & An, S.-I. (2009). Two types of El Niño events: Cold tongue El Niño and warm pool El Niño. *Journal of Climate*, *22*, 1499–1515. https://doi.org/10.1175/2008JCLI2624.1

30. Larkin, N. K., & Harrison, D. E. (2005). Global seasonal temperature and precipitation anomalies during El Niño autumn and winter. *Geophysical Research Letters, 32,* 705. https://doi.org/10.1029/2005GL022860

31. Lau, K. M., Wu, H. T., & Bony, S. (1997). The role of large-scale atmospheric circulation in the relationship between tropical convection and sea surface temperature. *Journal of Climate, 10,* 381–392. https://doi.org/10.1175/1520-0442(1997)010<0381:TROLSA>2.0.CO;2

32. Le Quéré, C., Andrew, R. M., Canadell, J. G., Sitch, S., Korsbakken, J. I., Peters, G. P., et al. (2016). Global Carbon Budget 2016. *Earth System Science Data, 8,* 605–649. https://doi.org/10.5194/essd-8-605-2016

33. Lim, Y., Kovach, R. M., Pawson, S., & Vernieres, G. (2017). The 2015/16 El Niño Event in Context of the MERRA-2 Reanalysis: A Comparison of the Tropical Pacific with 1982/83 and 1997/98. *Journal of Climate, 30,* 4819–4842, https://doi.org/10.1175/JCLI-D-16-0800.1

34. Liu, J., Bowman, K. W., Schimel, D. S., Parazoo, N. C., Jiang, Z., Lee, M., et al. (2017a). Contrasting carbon cycle responses of the tropical continents to the 2015–2016 El Niño. *Science,* 358, eaam5690. https://doi.org/10.1126/science.aam5690

35. Liu, L., Yang, G., Zhao, X., Feng, L., Han, G., Wu, Y., & Yu, W. (2017b). Why was the Indian Ocean Dipole weak in the context of the extreme El Niño in 2015? *Journal of Climate, 30,* 4755–4761. https://doi.org/10.1175/JCLI-D-16-0281.1

36. Page, S. E., Siegert, F., Rieley, J. O., Boehm, H.-D. V., Jaya, A., & Limin, S. (2002). The amount of carbon released from peat and forest fires in Indonesia during 1997. *Nature, 420,* 61–65. https://doi.org/10.1038/nature01131

37. Pan, X., Chin, M., Ichoku, C. M., & Field, R. D. (2018). Connecting Indonesian fires and drought with the type of El Niño and phase of the Indian Ocean dipole during

1979–2016. *Journal of Geophysical Research: Atmospheres*, *123*, 7974–7988. https://doi.org/10.1029/2018JD028402

38. Park, J.-H., Kug, J.-S., Li, T., & Behera, S. K. (2018). Predicting El Niño Beyond 1-year Lead: Effect of the Western Hemisphere Warm Pool. *Scientific Reports*, *8*, 14957. https://doi.org/10.1038/s41598-018-33191-7
39. Rayner, N., Parker, D. E., Horton, E., Folland, C., Alexander, L., Rowell, D., et al. (2003). Global analyses of sea surface temperature, sea ice, and night marine air temperature since the late nineteenth century. *Journal of Geophysical Research: Atmospheres*, *108*(D14), 4407. https://doi.org/10.1029/2002JD002670
40. Saji, N. H., Goswami, B. N., Vinayachandran, P. N., & Yamagata, T. (1999). A dipole mode in the tropical Indian Ocean. *Nature*, *401*(6751), 360–363. https://doi.org/10.1038/43854
41. van der Werf, G. R., Dempewolf, J., Trigg, S. N., Randerson, J. T., Kasibhatla, P. S., Giglio, L., et al. (2008). Climate regulation of fire emissions and deforestation in Equatorial Asia. *Proceedings of the National Academy of Sciences of the United States of America*, *105*, 20350–20355. https://doi.org/10.1073/pnas.0803375105
42. van der Werf, G. R., Randerson, J. T., Collatz, G. J., Gigio, L., Kasibhatla, P. S., Arellano Jr., A. F., et al. (2004). Continental-scale partitioning of fire emissions during the 1997 to 2001 El Niño/La Niña period. *Science*, *303*, 73–76. https://doi.org/10.1126/science.1090753
43. van der Werf, G. R., Randerson, J. T., Giglio, L., van Leeuwen, T. T., Chen, Y., Rogers, B. M., et al. (2017). Global fire emissions estimates during 1997–2016. *Earth System Science Data*, *9*, 679–720. https://doi.org/10.5194/essd-9-697-2017
44. Waliser, D. E., & Graham, N. (1993). Convective cloud systems and warm pool sea surface temperatures: Coupled interactions and self-regulation. *Journal of*

*Geophysical Research: Atmospheres*, *98*, 12881–12893. https://doi.org/10.1029/93JD00872

45. Wang, B., Luo, X., Yang, Y.-M., Sun, W., Cane, M. A., Cai, W., et al. (2019). Historical change of El Niño properties sheds light on future changes of extreme El Niño. *Proceedings of the National Academy of Sciences of the United States of America*, *116*, 22512–22517. https://doi.org/10.1073/pnas.1911130116
46. Wang, J., Zeng, N., Wang, M., Jiang, F., Wang, H., & Jiang, Z. (2018). Contrasting terrestrial carbon cycle responses to the 1997/98 and 2015/16 extreme El Niño events. *Earth System Dynamics*. *9*, 1–14. https://doi.org/10.5194/esd-9-1-2018
47. Weng, H., Ashok, K., Behera, S. K., Rao, S. A., & Yamagata, T. (2007). Impacts of recent El Niño Modoki on dry/wet conditions in the Pacific Rim during boreal summer. *Climate Dynamics*, *29*, 113–129. https://doi.org/10.1007/s00382-007-0234-0
48. Weng, H., Behera, S. K., & Yamagata, T. (2009). Anomalous winter climate conditions in the Pacific rim during recent El Niño Modoki and El Niño events. *Climate Dynamics*, 32, 663–674. https://doi.org/10.1007/s00382-008-0394-6
49. Wooster, M. J., Perry, G. L. W., & Zoumas, A. (2012). Fire, drought and El Niño relationships on Borneo (Southeast Asia) in the pre-MODIS era (1980–2000). *Biogeosciences*, *9*, 317–340. https://doi.org/10.5194/bg-9-317-2012
50. Xie, P. P., & Arkin, P. A. (1997). Global precipitation: a 17-year monthly analysis based on gauge observations, satellite estimates, and numerical model outputs. *Bulletin of the American Meteorological Society*, *78*, 2539–2558. https://doi.org/10.1175/1520-0477(1997)078<2539:GPAYMA>2.0.CO;2
51. Xie, S.-P., & Philander, S. G. H. (1994). A coupled ocean-atmosphere model of relevance to the ITCZ in the eastern Pacific. *Tellus A: Dynamic Meteorology and Oceanography*, *46*, 340–350. https://doi.org/10.3402/tellusa.v46i4.15484

52. Yin, Y., Ciais, P., Chevallier, F., van der Werf, G. R., Fanin, T., Broquet, G., et al. (2016). Variability of fire carbon emissions in Equatorial Asia and its nonlinear sensitivity to El Niño. *Geophysical Research Letters*, *43*, 10472–10479. https://doi.org/10.1002/2016GL070971

53. Zhang, T., Yang, S., Jiang, X., & Huang, B. (2016). Roles of remote and local forcings in the variation and prediction of regional Maritime Continent rainfall in wet and dry seasons. *Journal of Climate*, *29*, 8871–8879. https://doi.org/10.1175/JCLI-D-16-0417.1

Table 1. Correlation between burned area in Equatorial Asia and SSTA-based indices in October

| Month | Burned Area in Equatorial Asia | Correlation | Partial correlation without Niño3.4 | Partial correlation without DMI | Partial correlation without local SST |
|---|---|---|---|---|---|
| October | Niño3.4 | 0.73** | | 0.52* | 0.39 |
| | DMI | 0.75** | 0.57** | | 0.23 |
| | Local SST | 0.79** | 0.56** | 0.40 | |
| September | Niño3.4 | 0.85** | | 0.80** | 0.66** |
| | DMI | 0.67** | 0.53** | | 0.20 |
| | Local SST | 0.77** | 0.41 | 0.53* | |

* for $P<0.05$ and ** for $P<0.01$

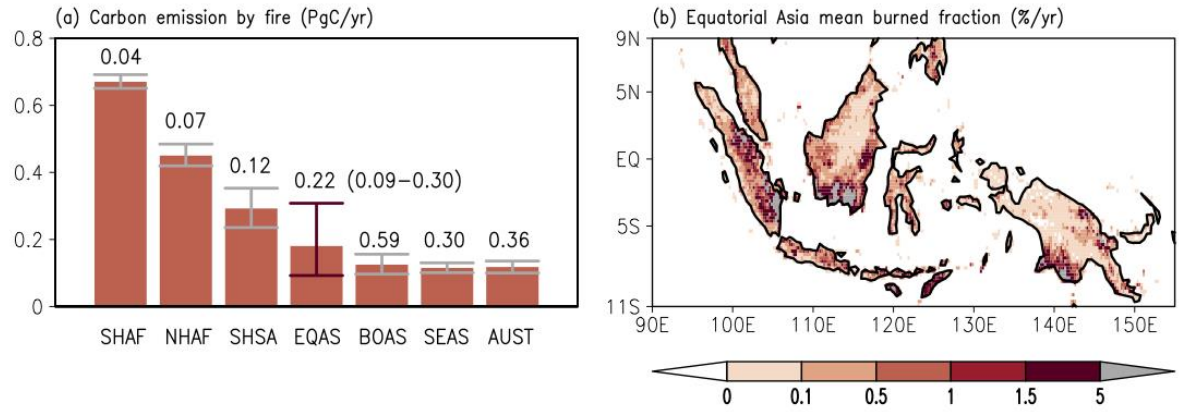


**Figure 1.** (a) Mean carbon emission by fire (bar) for Southern Hemisphere Africa (SHAF), Northern Hemisphere Africa (NHAF), Southern Hemisphere South America (SHSA), Equatorial Asia (EQAS), Boreal Asia (BOAS), Southeast Asia (SEAS) and Australia and New Zealand (AUST) over 1997–2015 from the fourth version of Global Fire Emissions Database and error bars and numbers are 95% significance ranges of mean carbon emission by fire based on the bootstrap method with 10,000 times resampling to estimate mean value (PgC $yr^{-1}$). (b) Mean burned fraction over Equatorial Asia for the period 1997–2015 (% $yr^{-1}$).

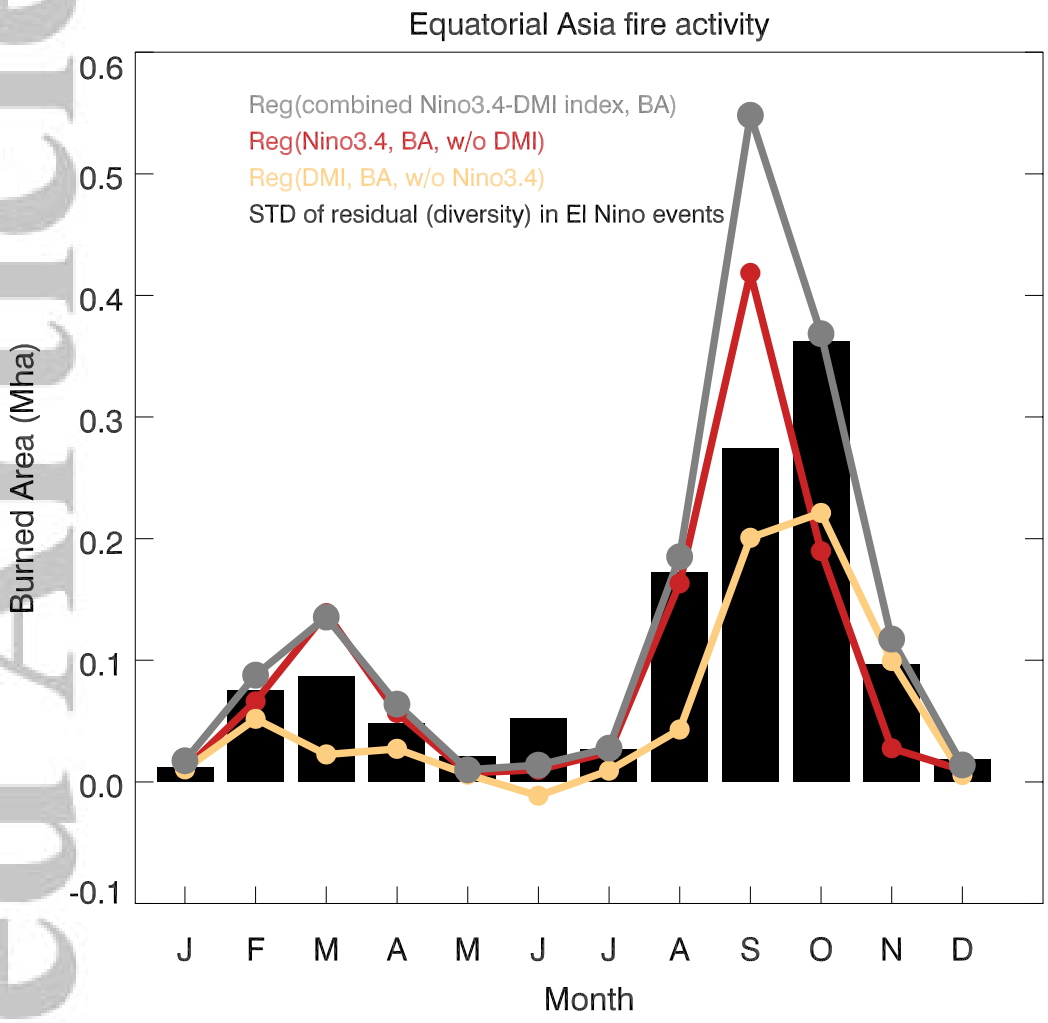


**Figure 2.** Fire activity in Equatorial Asia related to ENSO and IOD. Partial regression coefficients of burned area with normalized Niño3.4 as $\alpha$ in equation (1) (red), DMI as $\beta$ in equation (1) (yellow) on Equatorial Asian burned area. Gray line shows the summation of partial contributions with respect to normalized Niño3.4 and DMI, which are explained burned area by Niño3.4-DMI index. Standard deviation of residuals, $\varepsilon$ in equation (1), are shown in the black bars for recent seven El Niño events that are 1997, 2002, 2004, 2006, 2009, 2014 and 2015. Units are Mha.

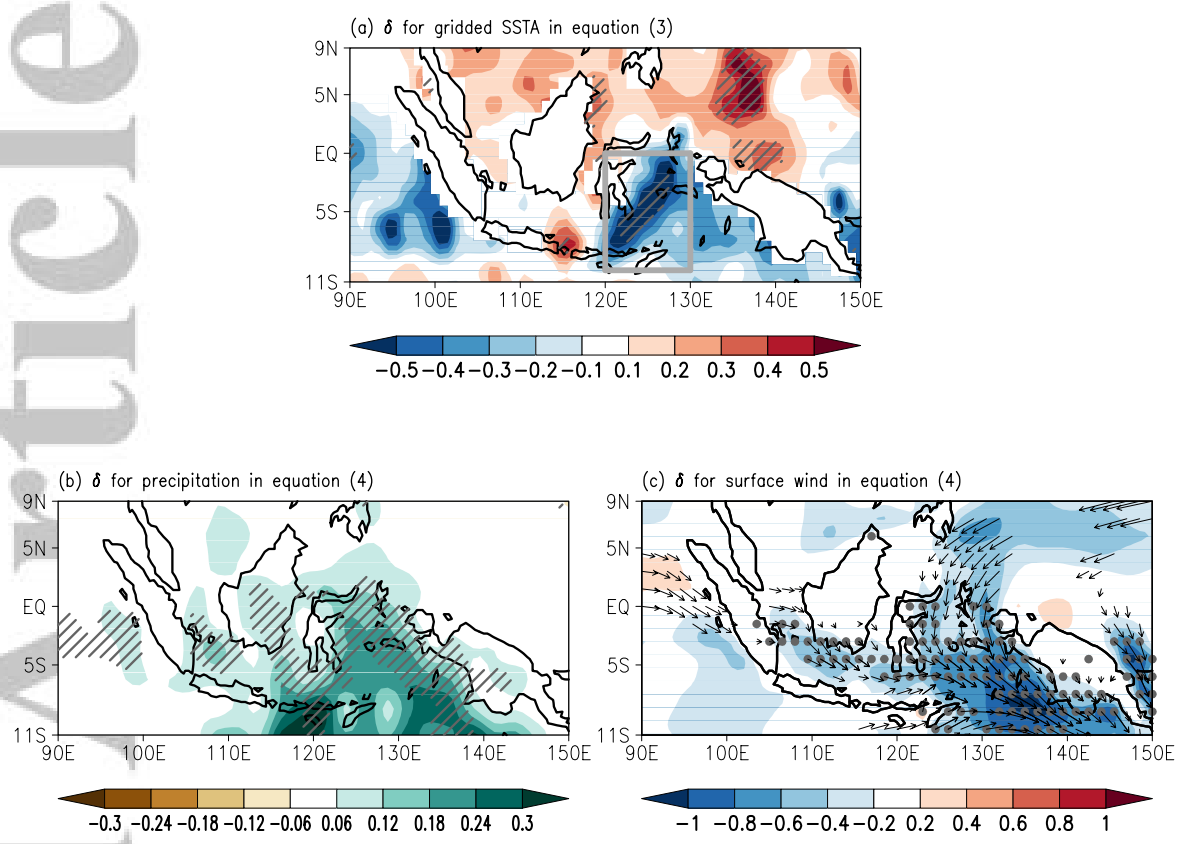


**Figure 3.** (a) Regression coefficients of gridded SST anomalies in October on the burned area over Equatorial Asia (90°–155°E, 11°S–9°N), excluding the influence of normalized Niño3.4-DMI index for the period 1995–2015. This is $\delta$ in equation (3). Unit is °C Mha$^{-1}$. (b) Regression coefficients of gridded precipitation anomalies (mm d$^{-1}$) on the SST over the Banda Sea (120°–130°E, 10°–0°S), the boxed area in (a), excluding the influence of normalized Niño3.4-DMI index for the period 1979–2015. This is $\delta$ in equation (4). (c) Regression coefficients of gridded surface wind anomalies (vector and dot) and wind speed (shaded; m s$^{-1}$) on the SST over the Banda Sea, excluding the influence of normalized Niño3.4-DMI index. This is $\delta$ in equation (4), but for wind. Hatching, wind vectors and dots are displayed only in significant regions at the 95% confidence level calculated using a Student's *t*-test.

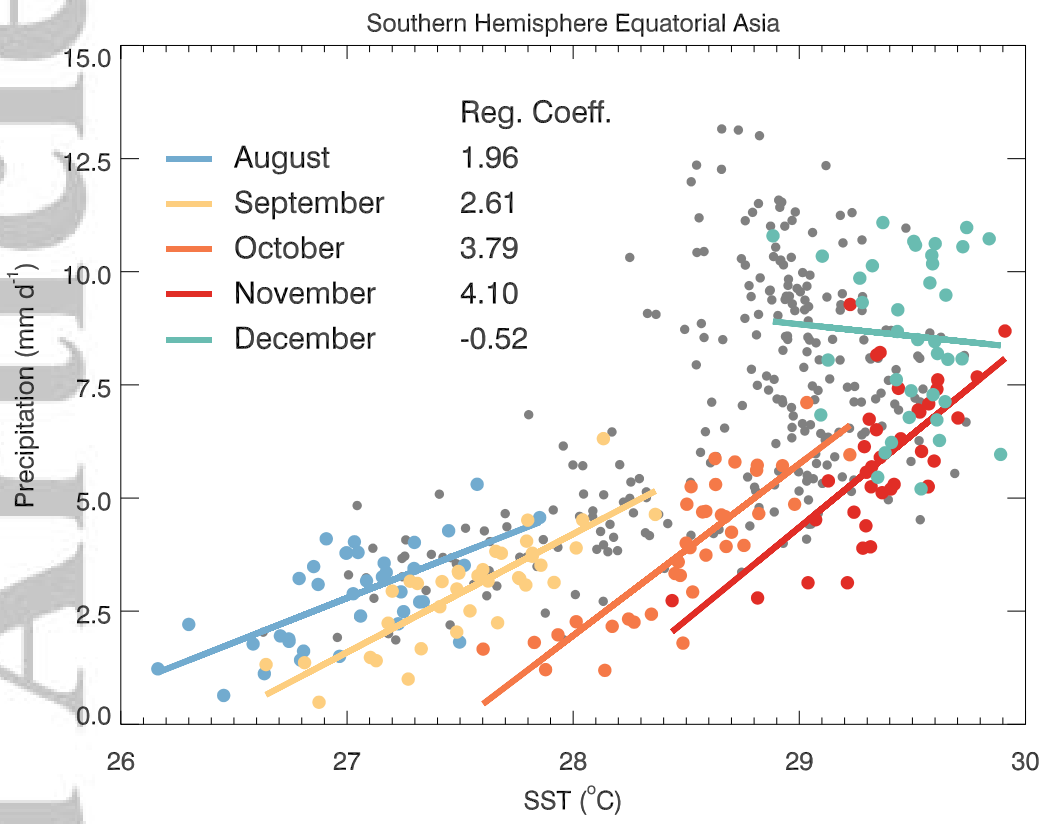


**Figure 4.** Precipitation (mm $d^{-1}$) over the Southern Hemisphere Equatorial Asia region (100°–150°E, 12°S–0°S) versus the local SST (°C) over the Banda Sea (120°–130°E, 10°–0°S). Color dots indicate dry season values from August to December and solid lines show the sensitivity of precipitation to the local SST.